Axisymmetric and Non-Axisymmetric Initiation of Vortex Breakdown

Andrew W. Cary

The Boeing Company
P.O. Box 516 MC S106-7126
St. Louis, MO 63166-0516, USA
andrew.w.cary@boeing.com

David L. Darmofal

Aeronautics & Astronautics
Massachusetts Institute of Technology
Cambridge, MA 02139, USA
darmofal@mit.edu

Abstract

The onset of axisymmetric (bubble) and non-axisymmetric (spiral) modes of breakdown is studied numerically for swirling pipe flows. We find that the onset of axisymmetric vortex breakdown occurs when the vortex attains local criticality. A transient simulation of the evolution of vortex breakdown revealed that downstream-running waves are trapped approximately at the location of flow criticality. These trapped waves are slowly amplified and eventually result in the bubble breakdown region with reversed flow and enlarged core size. Non-axisymmetric disturbance were found to decay on columnar base flows; however, for base flows with bubble breakdown, non-axisymmetric disturbances were amplified. These amplified disturbances resulted in the formation of spiral breakdown. If the base flow inlet swirl was only slightly larger than that leading to axisymmetric breakdown, a nearly columnar solution was obtained, suggesting that weak asymmetry may help to stabilize the columnar solution branch. The numerical simulations also revealed that most of the energy in spiral breakdown is contained in the first few non-axisymmetric modes of variation.

1 Introduction

Since first observed by Peckham and Atkins[1], the sudden transition of a concentrated vortex-dominated flow to a less coherent spiraling flow referred to as vortex breakdown has attracted considerable attention for both practical and theoretical reasons. The appearance of vortex breakdown over swept wings at high angles of attack imposes additional requirements on manuevering for these vehicles and can lead to significant design issues associated with increased fatigue on parts of an aircraft in its wake. The use of the recirculation region associated with vortex breakdown as a fluid dynamic flame holder in combustion engines provides a mechanism to increase the mixing between the fuel and the air without needing to decelerate the main flow as significantly as would otherwise be necessary, thereby increasing the efficiency of the engine.

Although there are two dominant modes for vortex breakdown, as many as seven different forms have been cataloged by Faler and Liebovich[2] and by Sarpkaya[3]. The "bubble" mode is predominantly axisymmetric in nature and is characterized by a recirculation region several times larger than the vortex core prior to breakdown. The "spiral" mode tends to be observed at lower swirl ratios than the bubble mode and is distinguished by a sharp bend in the vortex core, followed by the formation of several turns of a helix before losing its coherency. The different modes are sensitive to flow conditions and have often been observed to spontaneously transition from one mode to another. Brücker[4] used laser sheet visualization to more closely examine the transition between modes and identified the development of a rotating structure inside the recirculation zone of a bubble mode that tilted and

Paper presented at the RTO AVT Symposium on "Advanced Flow Management: Part A – Vortex Flows and High Angle of Attack for Military Vehicles", held in Loen, Norway, 7-11 May 2001, and published in RTO MP-069(I).

Report Documentation Page

Form Approved
OMB No. 0704-0188

1. REPORT DATE	2. REPORT TYPE	3. DATES COVERED
00 MAR 2003	**N/A**	**-**

4. TITLE AND SUBTITLE	5a. CONTRACT NUMBER
Axisymmetric and Non-Axisymmetric Initiation of Vortex Breakdown	5b. GRANT NUMBER
	5c. PROGRAM ELEMENT NUMBER
6. AUTHOR(S)	5d. PROJECT NUMBER
	5e. TASK NUMBER
	5f. WORK UNIT NUMBER
7. PERFORMING ORGANIZATION NAME(S) AND ADDRESS(ES) **NATO Research and Technology Organisation BP 25, 7 Rue Ancelle, F-92201 Neuilly-Sue-Seine Cedex, France**	8. PERFORMING ORGANIZATION REPORT NUMBER
9. SPONSORING/MONITORING AGENCY NAME(S) AND ADDRESS(ES)	10. SPONSOR/MONITOR'S ACRONYM(S)
	11. SPONSOR/MONITOR'S REPORT NUMBER(S)

12. DISTRIBUTION/AVAILABILITY STATEMENT
Approved for public release, distribution unlimited

13. SUPPLEMENTARY NOTES
Also see: ADM001490, Presented at RTO Applied Vehicle Technology Panel (AVT) Symposium held inLeon, Norway on 7-11 May 2001, The original document contains color images.

14. ABSTRACT

15. SUBJECT TERMS

16. SECURITY CLASSIFICATION OF:			17. LIMITATION OF ABSTRACT	18. NUMBER OF PAGES	19a. NAME OF RESPONSIBLE PERSON
a. REPORT	b. ABSTRACT	c. THIS PAGE			
unclassified	**unclassified**	**unclassified**	**UU**	**22**	

Standard Form 298 (Rev. 8-98)
Prescribed by ANSI Std Z39-18

extended to create the helix of the spiral mode as the swirl ratio was decreased. The reverse of this procedure occurred when the spiral mode transitioned to the bubble mode.

The main emphasis of this paper is to explore the connection between wave propagation and the onset of bubble and spiral modes of vortex breakdown. Squire[5] is generally credited with the first suggestion that vortex breakdown could be explained with concepts of wave motion. A central element of Squire's work (and most wave theories of vortex breakdown since Squire) is the division of vortical flows into supercritical and subcritical states. Supercritical vortices support only downstream-running waves while subcritical vortices support both downstream- and upstream-running waves. Experimental data shows that vortices without breakdown or upstream of breakdown are supercritical[6, 7, 8]. Squire proposed that vortex breakdown becomes possible when a vortex first achieves criticality. As discussed in numerous reviews[8, 9, 10, 11, 12], Squire suggested that disturbances that are present downstream could be transmitted upstream when a vortex achieves critical conditions, and these upstream-running disturbances would then be responsible for initiating vortex breakdown. Thus, according to Squire's hypothesis, vortical flows at the onset of breakdown should attain critical conditions at some location along the vortex core. Benjamin[13, 14] advocated a similar argument based on the existence of conjugate flow states at the breakdown location.

Recent theoretical and computational work has resulted in significant progress in the understanding of axisymmetric breakdown. Randall and Leibovich[15] used a weakly nonlinear analysis to show that the steady, Euler equations contain a solution branch which bifurcates from the columnar vortex solution at the critical swirl. This branch of solutions is characterized by a standing solitary wave which evolves from a columnar, swirling base flow in an infinitely long, straight pipe. Leibovich and Kribus[16] have extended this to larger amplitudes and show that a stagnation point can develop in the solitary wave.

Beran and Culick[17] have solved the steady, axisymmetric Navier-Stokes equations in pipes of varying-area and revealed a more complicated bifurcation picture. Specifically, for sufficiently high Reynolds number, they found the existence of two limit points. As shown in Fig. 1, limit point A marks the end of the near columnar solution branch and is the highest value of swirl for which a columnar steady solution was found. Above this swirl, the solution jumps to the lower branch which contains bubble breakdown with large regions of reversed flow. Limit point B marks the end of the breakdown solution branch. For lower swirls, the solutions must return to the columnar state. In between the two limit points, the solutions contain a localized standing wave which gradually merges with the other branches. More recent analysis has shown this localized standing wave branch to be unstable[18, 19].

Although Beran and Culick did not possess definitive proof, they suggested that limit point A corresponds to the occurrence of critical conditions in the flow. Specifically, they solved Hall's[10, 20] quasi-cylindrical equations and showed that numerical integration of these equations fail at approximately the same inlet swirl as limit point A in the full Navier-Stokes simulations. Since Hall[10] has shown that the quasi-cylindrical equations fail at the critical state, Beran and Culick hypothesized that limit point A corresponds to the occurrence of criticality in the flow, and, thus, is equivalent to the bifurcation described by Randall and Leibovich. One contribution of this paper is to show that this limit point does indeed coincide with the occurrence of local flow criticality.

In a recent series of papers by Wang and Rusak[21, 22, 23, 24], significant advances have been made to unify, in a solid theoretical foundation, the various studies of axisymmetric vortex breakdown. Their basic approach is to study the stability of columnar solutions of the Euler equations in a finite length, constant area pipe and connect the stability results to the time asymptotic solutions supported in the pipe. In their theoretical analysis, they find a bifurcation diagram similar to that of Beran and Culick's numerical study. According to their theory, limit point A occurs at the equivalent of Squire's

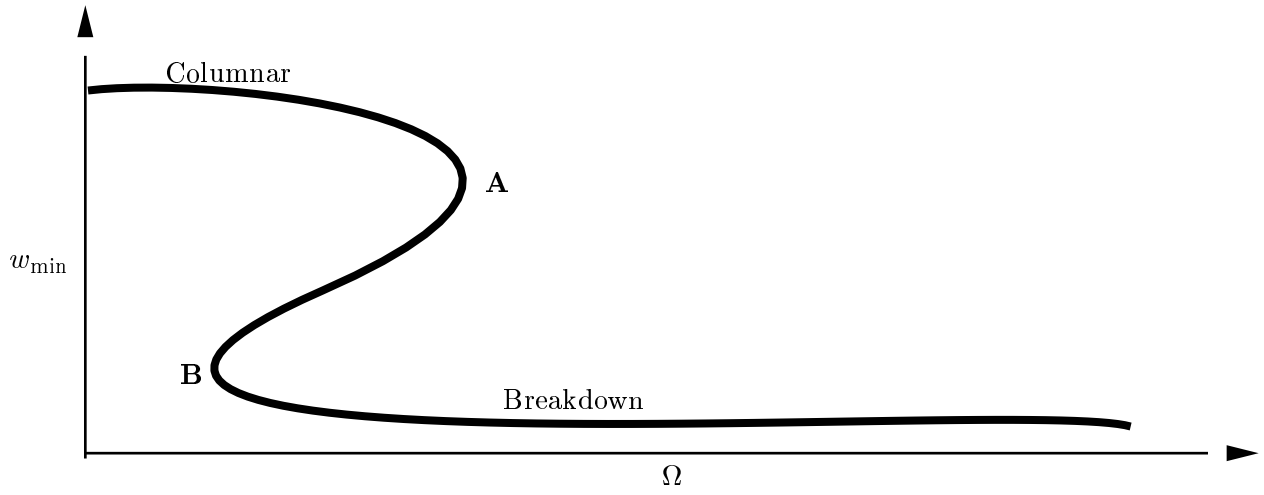

Figure 1: Minimum axial velocity, $w_{\min}$ for steady solutions of the Navier-Stokes equations versus inlet swirl, Ω, as observed by Beran and Culick[17].

or Benjamin's critical state for a finite length pipe. Above the critical swirl, the columnar solutions are unstable and the breakdown branch must be observed as the time-asymptotic state. Limit point B is equivalent to Escudier and Keller's two-stage transition model[25] of vortex breakdown which features a hollow breakdown region with stagnant flow. In numerical simulations of the unsteady, Euler equations[26], they confirm their analysis and show that finite amplitude disturbances can result in a columnar solution developing into a breakdown solution.

The remainder of the paper proceeds as follows. First, we concentrate on axisymmetric pipe flows and use numerical simulations to investigate the onset of bubble breakdown. In particular, we show that the onset of bubble breakdown coincides with local flow criticality. Then, we consider non-axisymmetric disturbances on axisymmetric base flows and use transient simulations to study the onset of spiral breakdown. The simulations show that the non-axisymmetric disturbances do not grow until bubble breakdown is present in the axisymmetric base flow. In addition, we show that the majority of the energy content of spiral breakdown is contained in the first few non-axisymmetric modes.

2 Axisymmetric Flow

We begin by analyzing the criticality of ten different pipe flow trials which have been simulated using an axisymmetric Navier-Stokes solver. The algorithm used to calculate the incompressible, swirling flow is a finite volume discretization described in detail in Darmofal[27]. The solver has been validated with numerous comparisons to both experiments and computations by other investigators[27]. Of specific interest to this work, the solver has been used to show that axisymmetric simulations provide good quantitative agreement with experimental results for bubble breakdown in swirling pipe flows[28].

A single trial for a given pipe flow consists of starting with a zero inlet swirl steady flow and quasi-statically raising the inlet swirl until breakdown occurs at a swirl of Ω_b. The criticality is determined by solving an appropriate eigenvalue problem as described by Benjamin[13] and in a more approximate manner using a local mean swirl number similar to Spall[29], Robinson, *et al.*[30], and Delery[12]. The eigenvalue criticality calculation assumes the flow can be analyzed using locally periodic eigenmodes and thus requires small axial gradients. Since the eigenvalue analysis is conducted on only smooth,

Pipe	z_t	z_o	z_c	$z_{\max}$	R_i	R_t	R_o	R_c
A	5	10	25	30	2.0	1.8	2.0	1.8
B	5	10	25	30	2.0	1.8	2.4	1.8

Pipe	z_i	z_d	z_t	$z_{\max}$	R_i	R_t	R_c
C	3.4	70	75	80	5.0	6.67	5.0
D	3.4	37	42	47	5.0	5.84	5.0

Table 1: Constants for pipe geometries

nearly columnar flows, these conditions can generally be satisfied. Our results show conclusively that the limiting swirl at which breakdown occurs coincides with the occurrence of local flow criticality as suggested by both Beran and Culick and by Wang and Rusak.

The inlet boundary conditions model the incoming flow as a q-vortex[8, 31]. Specifically,

$$\begin{aligned} u(r, z=0) &= 0, \\ \Gamma(r, z=0) &= \Omega\left[1-\exp(-r^2)\right], \\ w(r, z=0) &= 1+\Delta w \exp(-r^2). \end{aligned} \tag{1}$$

Velocities are non-dimensionalized by W_∞, the free stream axial velocity. The circulation function is defined as $\Gamma = rv$ and the value of q as defined by Batchelor[31] is $q = \Omega/\Delta w$. The vortex core size, δ, is used as a length scale. Therefore, $r = 1$ is the core edge, even though the maximum swirl occurs at $r = 1.21$. The pipe wall is modeled as an inviscid, slip boundary in order to avoid any ambiguities associated with wall boundary layer behavior. Finally, at the outlet, the flow is assumed to have negligible axial gradients and all axial derivatives are approximated by one-sided differences. For all of the axisymmetric results in this paper, the Reynolds number, $Re = W_\infty \delta/\nu$, is set to 1000. We have found no substantial variations in flow characteristics for Reynolds numbers above about 500[27].

Two different pipe geometries have been studied in this paper. The first possesses a converging-diverging inlet section, a constant area test section, and converging outlet section; it is a slight variant of the geometry considered by Beran and Culick[17]. The inlet section serves to isolate the inlet boundary from the breakdown bubble which occurs in the diverging section of the pipe. The specific pipe radius, $R(z)$, chosen for this investigation is

$$R(z) = \left\{ \begin{array}{ll} R_i + (R_t - R_i) g(z, z_t), & 0 < z < z_t \\ R_t + (R_o - R_t) g(z - z_t, z_o - z_t), & z_t < z < z_o \\ R_o, & z_o < z < z_c \\ R_o + (R_c - R_o) g(z - z_c, z_{\max} - z_c), & z_c < z < z_{\max} \end{array} \right\}, \tag{2}$$

$$g(z, l) = \frac{1}{2}\left\{1 - \cos[\pi(z/l)]\right\}.$$

Specific constants for the two pipes (A and B) with this basic form are given in Table 1. Note that Pipe B has a larger area increase than Pipe A.

The second geometry was used in the experiments of Sarpkaya[3, 32, 33] and Leibovich *et al.*[2, 6, 34]. This pipe consists of a constant area inlet of radius R_i and length z_i, a divergence section from $z_i < z < z_d$ with a linear pipe radius variation, a constant area test section from $z_d < z < z_t$ with radius

Trial	Pipe	Fixed Δw value	Ω_b
1	A	$\Delta w = 0.0$	1.51
2	A	$\Delta w = 0.4$	1.97
3	B	$\Delta w = 0.0$	0.91
4	B	$\Delta w = 0.4$	1.38

Trial	Pipe	Fixed q value	Ω_b
5	A	$q = 1.8$	3.91
6	B	$q = 1.6$	2.92
7	B	$q = 1.8$	2.41
8	B	$q = 2.0$	2.10
9	C	$q = 1.8$	1.66
10	D	$q = 1.8$	2.15

Table 2: Trial definitions and Ω_b values

R_t, and a converging outlet section from $z_t < z < z_{\max}$. The specific form of the converging outlet section was not given in the references so we employ the same sinusoidal variation used in the outlet sections of Pipes A and B. We consider two pipes (C and D) with specific constants given in Table 1. Both pipes have the same divergence angle as that used in the previous experiments. Pipe C has the full length of the divergent section used in the experiments while Pipe D has approximately half the length. As we show below, while the quantitative details are different for these pipes, the qualitative results are unchanged. Also, both pipes feature a constant area test section which is significantly shorter than that in the experiment; again, this change should only affect the quantitative details.

The inlet radius of both Pipes C and D is 5.0δ which, when using the q-vortex for the inlet condition, implies the maximum swirl occurs at $0.242R_i$. This was chosen to provide a realistic comparison with the previous experiments. For example, Leibovich and Faler[2] present velocity profiles with the location of maximum swirl ranging from approximately 1/4 to 1/3 of the pipe radius.

In all simulations, the axial grid spacing was $\Delta z = 0.2$. For Pipes A and B, the radial distribution of points, r_j, was constant at a given axial location,

$$r_j = R(z)\frac{j-1}{j_{\max}-1},$$

with $j_{\max} = 31$. The radial distribution of points for Pipes C and D was designed to decrease resolution outside the region where the core was expected and satisfied,

$$r_j = f_c R(z)\frac{j-1}{j_c-1},$$

for $1 < j \leq j_c$, and

$$r_j = R(z)\left[f_c + (1-f_c)\left(\frac{j-j_c}{j_{\max}-j_c}\right)^c\right]$$

for $j_c < j \leq j_{\max}$. Specifically, we used $f_c = 0.4$, $j_c = 31$, $j_{\max} = 51$, and $c = 1.27$. The cluster parameter, c, was chosen such that the first cell outside of the equally-spaced core region was approximately the same size as the cells in the core region.

As described above, ten trials were run varying the inlet swirl, Ω, in a quasi-static manner. In these trials, either the value of Δw or q is held constant at the inlet. The first solution of a trial is found by starting from an undisturbed flow with zero swirl. After finding the steady state solution, Ω is raised and the solution is again converged. The trial is complete when breakdown first occurs at the onset swirl, Ω_b. The value of Ω_b is determined to the nearest hundredth. The specifics of the ten trials described in this paper and the resulting onset swirls are presented in Table 2.

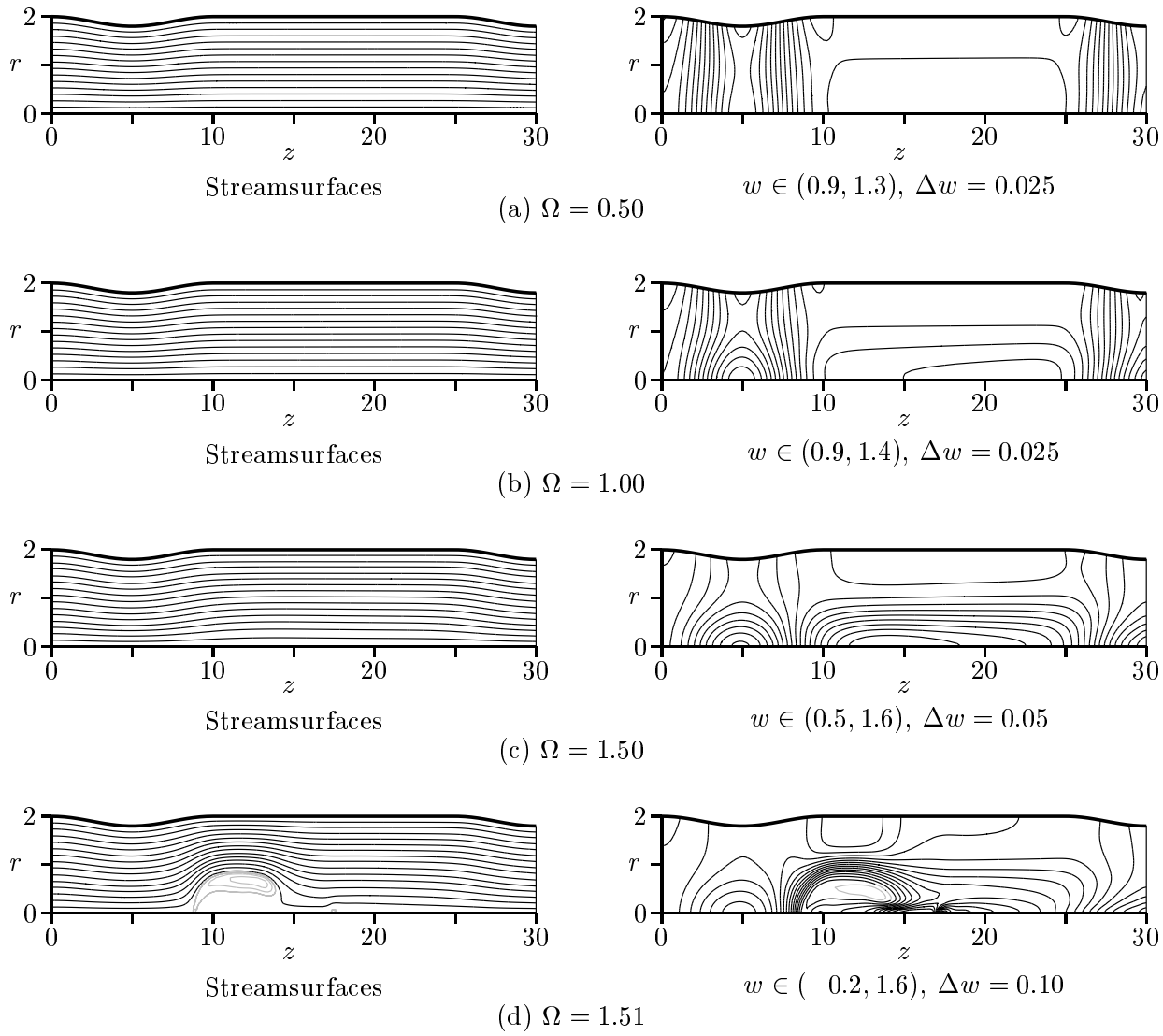

Figure 2: Streamsurfaces and axial velocity contours for Trial 1 axisymmetric steady solutions. $Re = 1000$.

Sample streamsurfaces and axial velocity contours from four steady solutions of Trial 1 are shown in Figure 2. For this trial, $\Omega_b = 1.51$. The streamsurfaces and the axial velocity contours for the solutions with $\Omega < \Omega_b$ show no indication of the impending breakdown at $\Omega = \Omega_b$. Although the minimum axial velocity is decreasing with increasing swirl, the flow is not near stagnation for $\Omega = 1.50$. An important point to notice is that even the flows which are on the verge of breakdown, such as $\Omega = 1.50$, are still smoothly varying. This provides some assurance that the criticality analysis in the following section is not flawed by the presence of large axial variations. The smoothness of the flows is especially true in the constant area section of the pipe which will be the first location to achieve critical conditions. Finally, as discussed by Beran and Culick[17], the drastic change in solution behavior is a result of the solution reaching a limit point in the solution space and jumping to the steady solutions with breakdown. In the next section, we will show that the limit point and corresponding jump is a result of the vortex becoming locally critical. Although we do not present any other streamsurface and

velocity plots, this sudden onset of vortex breakdown was characteristic of all ten trials.

2.1 Axisymmetric criticality analysis

For axisymmetric flows, it is possible to determine the criticality of a flow using a standing wave analysis[13]. To analyze standing waves, the vortex flow is divided into a steady, mean flow and a steady infinitesimal perturbation. The steady, mean flow velocity distribution is given by $[0, V(r,z), W(r,z)]$ and is assumed to have axial variations whose length scale, L, is large compared to the perturbation wavelength such that $|\gamma|L >> 1$. The streamfunction perturbation is defined as $\psi = f(r)\exp(\gamma z)$ where γ is the axial wavenumber. As given by Hall[10], the governing equation for stationary perturbations is:

$$r\frac{d}{dr}\left(\frac{1}{r}\frac{df}{dr}\right) + \left[\gamma^2 - \frac{r}{W}\frac{\partial}{\partial r}\left(\frac{1}{r}\frac{\partial W}{\partial r}\right) + \frac{1}{r^3W^2}\frac{\partial(\Gamma^2)}{\partial r}\right] f = 0, \tag{3}$$

where $\Gamma = rV(r,z)$ is the mean flow circulation. For flow in a pipe, the perturbation streamfunction is zero at $r = 0$ and at the pipe wall, $r = R(z)$. Hall[10] has shown that Eq. 3 is valid for quasi-cylindrical flows as well as columnar. An infinite, ordered set of eigenvalues exists for this Sturm-Liouville system such that $\gamma_0^2 < \gamma_1^2 < \gamma_2^2 < ...$[13]. Thus, the flow is supercritical when $\gamma_0^2 > 0$ since then all eigenvalues of Eq. 3 will be positive and only exponential solutions are possible. When $\gamma_0^2 < 0$, some perturbations are sinusoidally varying waves and the flow is subcritical. In the supercritical case, $|\gamma_0|$ gives the slowest decay rate of disturbances in the upstream direction and is a measure for how much a vortex will be influenced by downstream effects. For subcritical flows, $|\gamma_0|$ is the highest wavenumber possible for stationary waves on the mean flow.

In the following, the criticality of the 132 steady solutions from the 10 trials will be determined by calculating the local eigenvalues, γ^2, at each axial grid station for Eq. 3. The local mean flow is given by the local velocity distributions from the steady results of the axisymmetric, Navier-Stokes solver. The eigenvalues are calculated by discretizing Eq. 3 with a second order accurate finite difference scheme and using an EISPACK eigenvalue solver on the resulting matrix. For display purposes, only the value of γ_0^2 will be plotted since this eigenvalue completely determines the local criticality.

We have also examined some approximate criteria which are often used to determine whether or not breakdown is impending. Specifically, an increase of swirl ratio generally results in a decrease of vortex criticality from supercritical towards subcritical. Numerous authors[12, 29, 30] have investigated different techniques for evaluating the swirl ratio. For some unique swirl ratio, the vortex is assumed to become critical and vortex breakdown occurs. The previous studies have found that breakdown generally occurs for swirl numbers above approximately 1.4. While our technique for determining a local swirl ratio is again different from these references, the basic ideas are the same. We have tested the other suggestions for evaluating the local swirl and found the same basic trends as those we report using our method although our method seemed to provide the smallest range of maximum swirl ratios at breakdown onset. First, we define the local swirl number as $S = \Gamma_c/W_c r_c$ where Γ_c, W_c, and r_c are measures of the local circulation, core axial velocity, and core radius. We use the term swirl number instead of swirl ratio to avoid confusion with the inlet swirl ratio, Ω. The core radius at a particular axial station is determined by tracing the streamsurface which begins at the inlet location of maximum swirl velocity. For a given z location, the core radius, r_c, is the radial position of this streamsurface at z. The axial velocity, W_c, is the constant axial velocity required to conserve mass in the core. Finally, the local circulation is assumed to be equal to the inlet value, $\Gamma_c = \Omega$.

Figure 3 shows the axial distribution of γ_0^2, the centerline axial velocity, $w(0,z)$, and the swirl number, S for the Trial 1 flows with Ω = 1.48, 1.49, 1.50, and 1.51. Although we have calculated

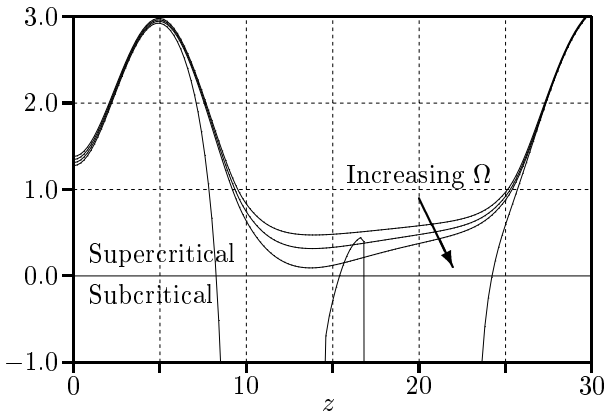

(a) Minimum eigenvalue, $\gamma_0^2(z)$

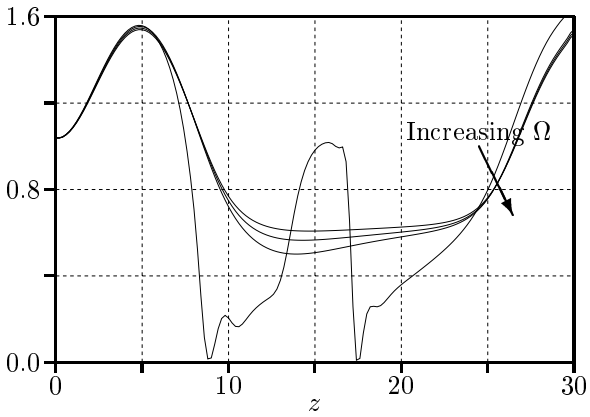

(b) Axial velocity at $r = 0$, $w(0, z)$

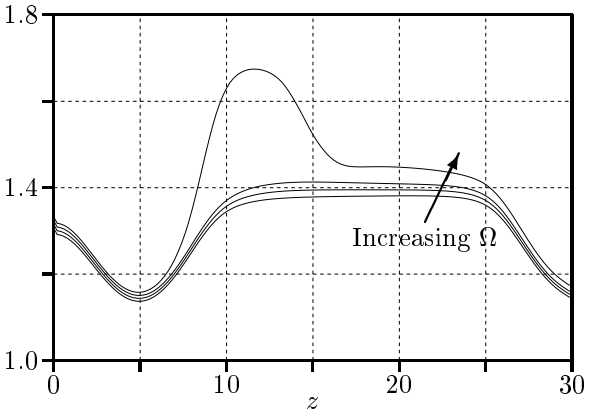

(c) Swirl number, $S(z)$

Figure 3: $\gamma_0^2(z)$, $w_0(0, z)$ and $S(z)$ distributions for Trial 1, $\Omega = 1.48$, 1.49, 1.50, and 1.51, $\Delta w = 0.0$.

the eigenvalues for the $\Omega = \Omega_b = 1.51$, they should not be interpreted too strongly because this flow contains breakdown and the large axial gradients surely invalidate the eigenvalue analysis within the vicinity of the breakdown region. As remarked in the previous section, the flows with $\Omega < \Omega_b$ are still smoothly varying and the eigenvalue analysis should be reasonably accurate. The results show that as the onset inlet swirl ratio is approached, the vortex is becoming locally critical at $z \approx 13$. For $\Omega = 1.50$, γ_0^2 is nearly zero. By contrast, the minimum centerline axial velocity is approximately 0.5 and far from stagnation for $\Omega = 1.50$. This highlights that vortex breakdown is not simply a stagnation process but rather that stagnation is a consequence of vortex breakdown.

Next, we plot the variation of the minimum eigenvalue, minimum centerline axial velocity, and maximum swirl number versus inlet swirl in Figure 4 for all 10 trials. The minimum eigenvalue, $\gamma_{0\,\min}^2$, and minimum centerline axial velocity, $w_{\min}$, are defined as the minimum value of these variables over all axial locations. The maximum swirl number, $S_{\max}$, is similarly defined. Figure 4 is a compilation of all of the data from From this figure, it is clear that the criticality as determined by $\gamma_{0\,\min}^2$ is a good indicator of impending vortex breakdown. The minimum eigenvalues of all of the columnar solutions with $\Omega = \Omega_b^-$ are nearly zero. By contrast, the swirl number, $S_{\max}$, is not as precise; breakdown occurs for values of $S_{\max}$ from approximately 1.2 to 1.8. While the swirl number may not be useful as a precise measure for the onset of vortex breakdown, it does appear to give the correct general trends.

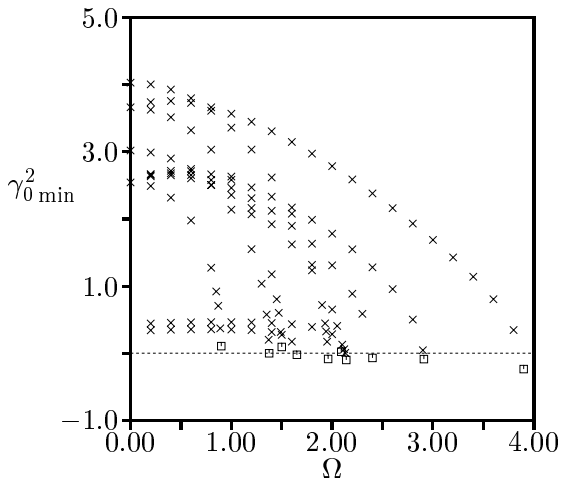

(a) Minimum eigenvalue, $\gamma^2_{0\,\min}$

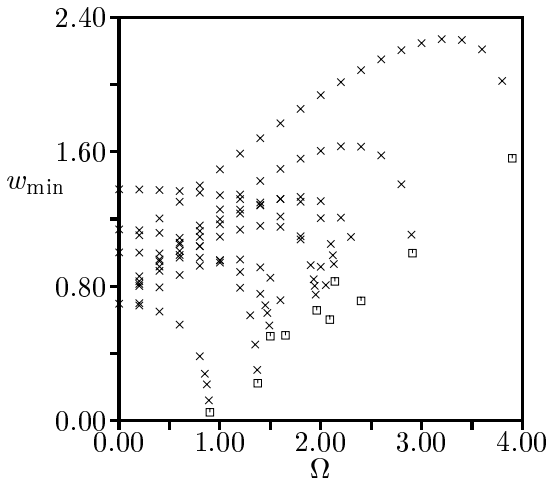

(b) Minimum axial velocity, $w_{\min}$

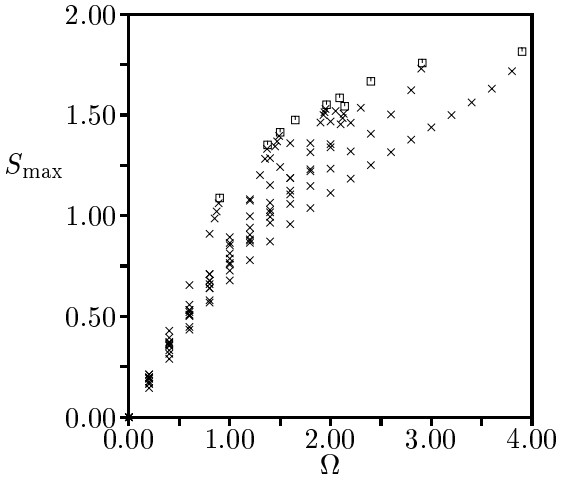

(c) Maximum swirl number, $S_{\max}$

Figure 4: $\gamma^2_{0\,\min}$, $w_{\min}$, and $S_{\max}$ versus Ω for all steady pipe flow solutions. $\times$, columnar solutions; $\square$, columnar solutions for which breakdown occurs if Ω is raised 1/100th (i.e. $\Omega_b = \Omega + 0.01$).

Specifically, $S_{\max}$ is a monotonically increasing function as breakdown approaches; thus, any effects which raise the local swirl number are likely to drive a flow closer to breakdown; similarly, effects which lower the local swirl number are likely to stabilize the flow away from vortex breakdown.

2.2 Transient formation of axisymmetric vortex breakdown

In this section, we report the results of a transient simulation of the formation of vortex breakdown. The initial flow is the steady result from Trial 1 for $\Omega = 1.50$. The inlet swirl ratio is then raised at $t = 0$ to $\Omega = 1.52$, initiating a disturbance which propagates throughout the domain. Since this swirl ratio is above that for which breakdown occurs ($\Omega_b = 1.51$), the final solution should contain breakdown and the transient will contain the breakdown evolution. Note, the solutions in this section were calculated with a timestep of approximately 0.041 δ/W_∞.

Figure 5 shows the streamsurfaces during the bubble evolution. At $t = 41$, only a slight per-

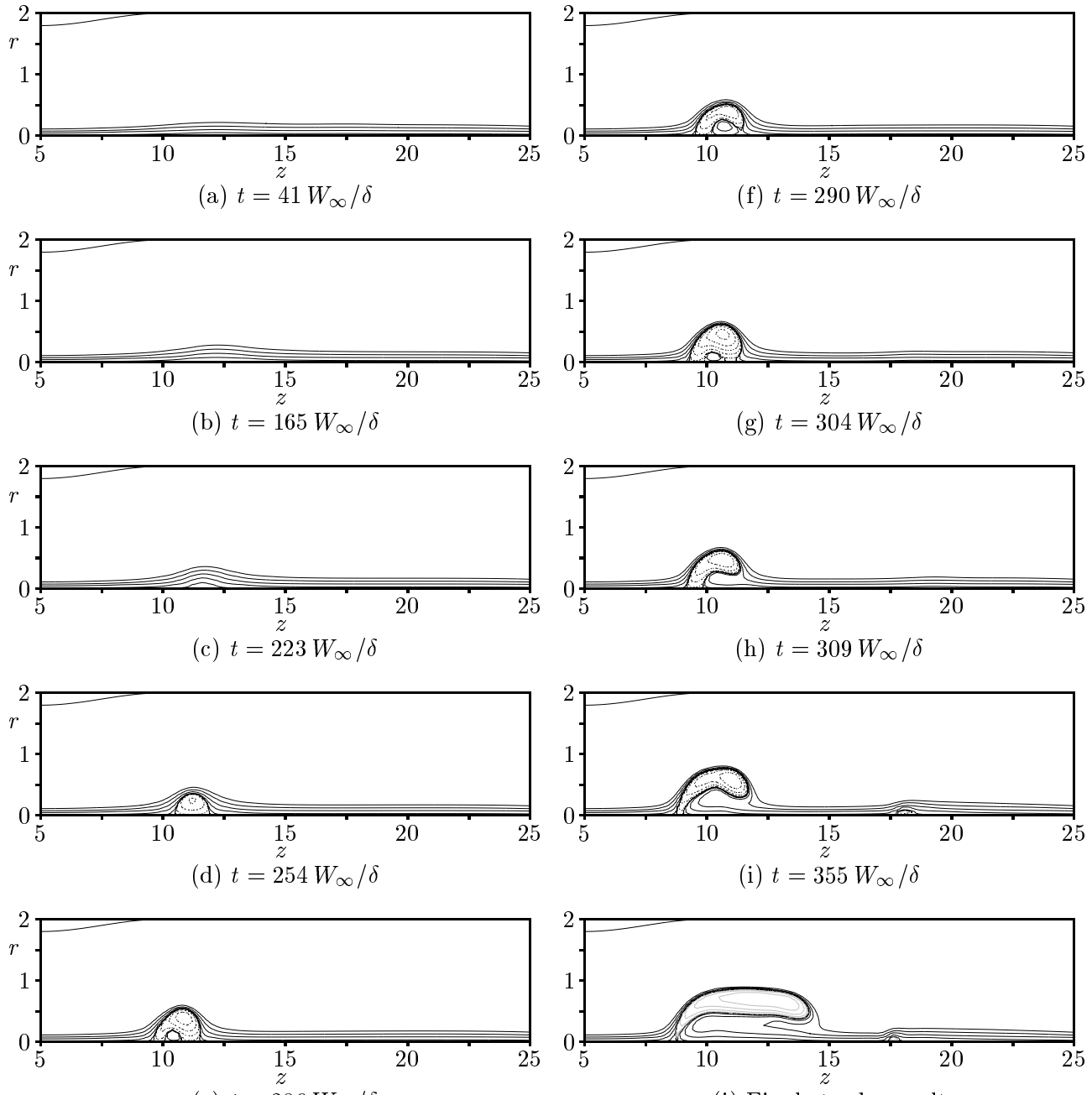

(a) $t = 41\,W_\infty/\delta$ (f) $t = 290\,W_\infty/\delta$

(b) $t = 165\,W_\infty/\delta$ (g) $t = 304\,W_\infty/\delta$

(c) $t = 223\,W_\infty/\delta$ (h) $t = 309\,W_\infty/\delta$

(d) $t = 254\,W_\infty/\delta$ (i) $t = 355\,W_\infty/\delta$

(e) $t = 286\,W_\infty/\delta$ (j) Final steady result

Figure 5: Transient bubble formation after change in inlet swirl from $\Omega = 1.50$ to 1.52 at $t = 0^+$. Pipe A, $\Delta w = 0.0$, $Re = 1000$.

turbation is visible at $z \approx 12.4$ By $t = 165$, the streamfunction perturbation has increased further, and, at $t = 223$, the $\Psi = 0$ streamsurface has lifted off the axis to form a small region of reversed flow. At $t = 254$, the bubble has become quite large and is moving upstream. The bubble formation from $t = 0$ to $t = 254$ is quite symmetric and strongly resembles the solitary wave solutions found by Leibovich[35], suggesting that the initial development of breakdown might be approximated by weakly nonlinear theory. At $t = 286$, an inner bubble is formed and the breakdown bubble loses its axial symmetry while continuing its upstream motion. As the breakdown evolution completes, the bubble takes on an open-ended shape, and, for $t = 355$, a second bubble forms at $z \approx 17.6$. Finally, the steady result, determined when the residual reached machine zero at approximately $t = 1300$, shows the first bubble has increased quite significantly in size and the second bubble has moved slightly upstream. Evidently, the unsteady bubble may be smaller than the final steady bubble structure. The calculation was continued for several thousand iterations after achieving steady state with no changes in the solution as shown in Fig. 5(l).

Escudier[9] describes an experimental breakdown evolution process and shows a time sequence of dye visualization photographs which are remarkably similar to the previous simulation results. In the experimental results, a slight swelling in the vortex core region initially appears just after a change in flow conditions. This swelling gradually develops into an initially axisymmetric ring-like structure. After some transient asymmetries, the structure stabilizes into a bubble breakdown structure slightly upstream of the initial swelling location with a second stagnation behind the primary bubble.

A useful technique to visualize the wave motion underlying the breakdown evolution is to track radial perturbations to the location of a particular streamfunction. For this purpose, we track the streamsurface, $\psi_{\max}$, which begins from the inlet at the location of maximum swirl. Perturbations to the streamfunction position are defined implicitly as,

$$\tilde{r}(z,t) = r(\psi_{\max}, z, t) - r(\psi_{\max}, z, 0).$$

Thus, regions of positive $\tilde{r}$ represent area for which the vortex core is growing. Figure 6 shows the evolution of $\tilde{r}$ after the increase in the inlet swirl. In part (a) of the figure, the initial stages of the development are shown. A small amplitude area-varying wave is emitted from the inlet and begins to propagate downstream. A portion of the disturbance propagates across the domain to the outlet; however, some of the disturbance is halted very near the location of flow criticality. As shown in parts (b) and (c) of the figure, this trapped wave continually amplifies and slowly moves upstream to its final position. Thus, one might interpret this breakdown formation as resulting from trapping and amplification of downstream-running disturbances at the critical location.

3 Asymmetric Disturbances

The assumption of axisymmetry provides a convenient simplification for theoretical development, but since physical flows are not bound by this constraint, theories must also be examined in the absence of this simplification. This section examines the behavior of a weak asymmetric disturbance on a steady axisymmetric base flow characterized by a given inlet swirl. We will be demonstrate that, until the base flow reaches a particular swirl ratio, the disturbance is passively convected and decays with minimal influence on the base flow. However, once the base flow achieves a critical state that would exhibit axisymmetric vortex breakdown, significant disturbance growth is predicted and large perturbations appear on the base flow. The basic mechanism for this growth is identified through consideration of the magnitude of the velocity components for each Fourier mode.

A psuedo-spectral method is used to simulate the flow by solving for the azimuthal Fourier modes of the velocity. This approach is more efficient for computing the lower azimuthal modes that are dom-

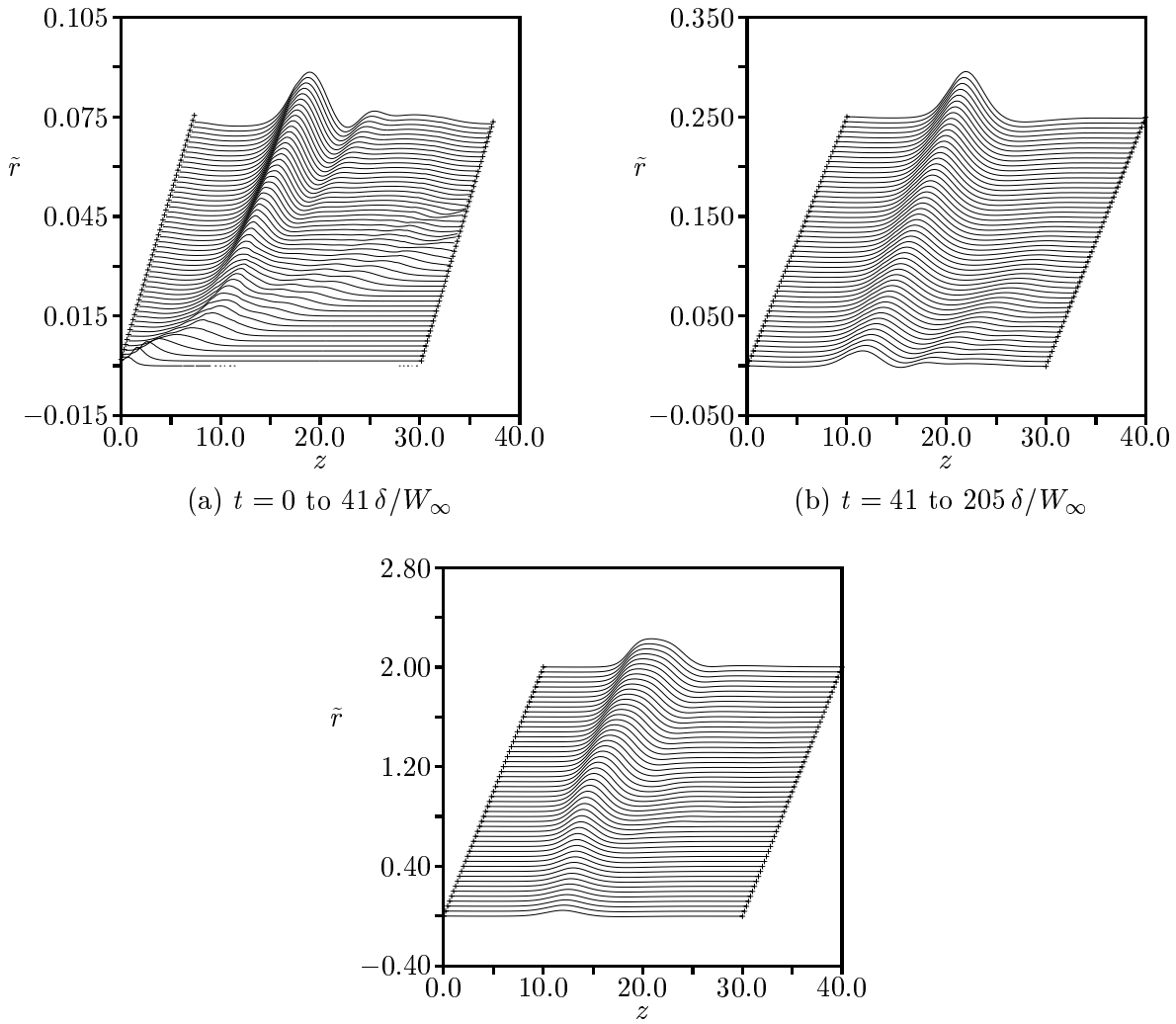

(a) $t = 0$ to $41\,\delta/W_\infty$

(b) $t = 41$ to $205\,\delta/W_\infty$

(c) $t = 205$ to $533\,\delta/W_\infty$

Figure 6: Transient evolution of the radial perturbation, $\tilde{r}$, of the maximum swirl streamline, $\psi_{\max}$ after raising inlet swirl from $\Omega = 1.50$ to 1.52.

inant in experiments and parallels theoretical techniques for investigating the flow. Furthermore, by using the Fourier-decomposed model, an axisymmetric solution can be maintained until asymmetries are deliberately introduced. The Fourier-decomposition of the velocity field is specified by

$$\mathbf{u} = \mathbf{U}(r,z) + \mathbf{u}_0(r,z,t) + \sum_{m=1}^{N_\theta} \left(\mathbf{u}_m(r,z,t) e^{-\imath m\theta} + \bar{\mathbf{u}}_m(r,z,t) e^{\imath m\theta} \right), \tag{4}$$

where $\mathbf{U}(r,z)$ is a steady axisymmetric base solution and an overbar $(^-)$ denotes complex conjugation. Thus $\mathbf{u}_m = u_m \mathbf{e}_r + v_m \mathbf{e}_\theta + w_m \mathbf{e}_z$ is a complex function of r z, and t representing the mth azimuthal mode of the perturbation velocity. The continuity and unsteady incompressible Navier-Stokes equations are written in cylindrical coordinates and Fourier-decomposed in the azimuthal direction to obtain a sequence of coupled partial differential equations. The system is discretized through the use of Chebyshev collocation in the radial direction and finite-differencing in the axial direction. The

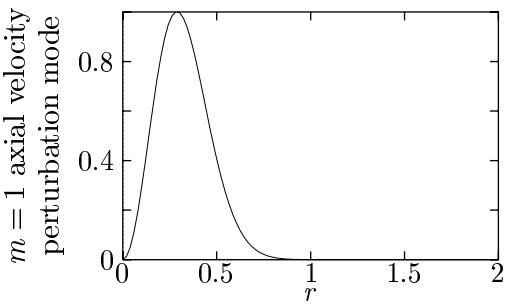

Figure 7: Radial distribution of axial velocity perturbation mode.

solution is obtained using an operator split approach that successively integrates the flow in time by performing a non-linear advection step, a pressure correction, and a viscous correction[36, 37].

As in the axisymmetric studies from the previous section, the flow is simulated in a converging-diverging nozzle with a slip wall boundary condition on the nozzle to prevent the interaction of the boundary layer with the breakdown. The inlet axisymmetric velocity distribution is specified using Eq. 1. Axis boundary conditions consistent with the Fourier-decomposition are used and the outflow is again parabolized using one-sided differences. A family of axisymmetric solutions are obtained using a modified Pipe A geometry that has had both the inlet section and the test section extended by 5 core radii and the final converging section removed. These changes were made to allow for the greater spatial extent of the anticipated solution. This family of solutions is similar to that obtained in Trial 1, but was computed at a lower Reynolds number of 500. Despite the significantly different numerical scheme, the axisymmetric solutions with the pseudo-spectral code showed very good comparison to results from the previous axisymmetric code[37].

Beginning with this family of axisymmetric base flows, a weak disturbance of the form

$$w_1(r, z = 0, t) = A(t) r^2 e^{-12r^2} \tag{5}$$

is introduced to the $m = 1$ mode of the axial velocity, where A is a measure of the amplitude that is linearly ramped in time to 1 percent of the inlet axial velocity. This perturbation, depicted in Fig. 7, is chosen to satisfy the boundary condition at the axis and to decay rapidly outside the vortex core. Amplitude values ranging from 0.05 to 5 percent of the inlet axial velocity have been simulated with similar qualitative results as those described below. As a consequence of the physical requirement for single-valued functions at $r = 0$, only the $m = 1$ mode can deflect fluid off the axis. Since this azimuthal mode can also stimulate all other azimuthal modes, it provides an effective means for introducing asymmetry into the flow.

3.1 Asymmetric disturbance growth

The minimum axial velocity on the axis is depicted in Fig. 8 for both the axisymmetric and asymmetric solutions as a function of inlet swirl. These results indicate that axisymmetric breakdown occurs at $\Omega_b = 1.48^+$. The small difference between this result and the previous axisymmetric Trial 1 is due to viscous effects, as confirmed by repeating Trial 1 at the lower Reynolds number.

The degree that the perturbation affects the flow can be evaluated by considering the integrated mode magnitude,

$$Q_m = \int_{\mathcal{V}} \frac{1}{2} \mathbf{u}_m \cdot \bar{\mathbf{u}}_m \, \mathrm{d}\mathcal{V}, \tag{6}$$

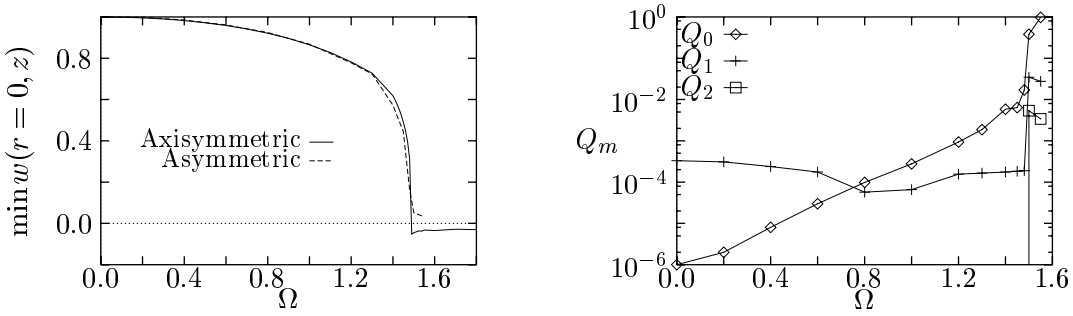

Figure 8: Variation of minimum axial velocity at $r = 0$ and Q_m versus inlet swirl. For asymmetric flows, a 1% $m = 1$ axial velocity perturbation is introduced.

where $\mathcal{V}$ is a radial slice through the nozzle. For the flows with axisymmetric inlet swirls less than that leading to breakdown, an asymmetric perturbation of the form given by Eq. 5 does not show significant amplification and decays with axial distance. This behavior is reflected in Fig. 8 which depicts the variation in Q_m with inlet swirl for the converged asymmetric solution. For a non-swirling flow, the disturbance propagates directly down the pipe. The addition of swirl both causes the disturbance to spiral as it travels downstream and shears the perturbation, increasing the dissipation rate. For these solutions, the weak asymmetry gradually decays and does not have any significant effect on the axisymmetric flow. As demonstrated by the small values of Q_m and by the agreement between the axisymmetric and asymmetric solution curves in Fig. 8, significant asymmetries do not develop until an inlet swirl of 1.49.

At $\Omega = 1.49$, the axisymmetric flow has just undergone vortex breakdown and a stagnation point has developed on the axis. In the cases predicted to have axisymmetric breakdown, the perturbation is amplified by several orders of magnitude, as depicted in Fig. 8, and leads to large changes in the flow field. These changes are also immediately evident in minimum axial velocity which indicates that the steady asymmetric solution does not develop a stagnation point on the axis even after the axisymmetric solution is predicting breakdown. While asymmetric solutions have been calculated in this geometry for swirl ratios up to 1.8, these higher swirl cases do not converge to a steady solution, but continue to have large, nearly periodic, oscillations for long non-dimensional times.

Evolution equations can be derived for the integrated mode magnitude Q_m by integrating the Navier-Stokes equations over the radial slice $\mathcal{V}$.

$$\frac{\mathrm{d}Q_0}{\mathrm{d}t} + \int (q_{00} + p_0) w_0 + q_{00} W \,\mathrm{dS}\Big|_{\text{inlet}}^{\text{outlet}} - \frac{1}{Re}\int_{\partial\mathcal{V}} \frac{\partial q_{00}}{\partial \mathbf{n}}\,\mathrm{dS}$$
$$= -\int_{\mathcal{V}} \left(\mathbf{u}_0\mathbf{u}_0 : \nabla_0 \mathbf{U} + 2\sum_{m=1}^{N_\theta} \mathbf{u}_0 \bar{\mathbf{u}}_m : \nabla_m \mathbf{u}_m + \frac{1}{Re}\nabla_0 \mathbf{u}_0 : \nabla_0 \mathbf{u}_0 \right) \mathrm{d}\mathcal{V} \quad (7)$$

$$\frac{\mathrm{d}Q_m}{\mathrm{d}t} + \int q_m(W+w_0) + \Re[\bar{w}_m(\mathbf{u}_0\cdot\mathbf{u}_m + p_m)]\,\mathrm{dS}\Big|_{\text{inlet}}^{\text{outlet}} - \frac{1}{Re}\int_{\partial\mathcal{V}} \frac{\partial q_m}{\partial \mathbf{n}}\,\mathrm{dS}$$
$$= -\Re\int_{\mathcal{V}} \Bigg(\bar{\mathbf{u}}_m\mathbf{u}_m : \nabla_0\mathbf{U} - \mathbf{u}_0\bar{\mathbf{u}}_m : \nabla_m\mathbf{u}_m + \sum_{j=1}^{m-1} \bar{\mathbf{u}}_m\mathbf{u}_j : \nabla_{m-j}\mathbf{u}_{m-j}$$
$$+ \sum_{j=1}^{N_\theta - m} (\mathbf{u}_m\bar{\mathbf{u}}_{m+j} : \nabla_j\mathbf{u}_j + \bar{\mathbf{u}}_m\bar{\mathbf{u}}_j : \nabla_{m+j}\mathbf{u}_{m+j}) + \frac{1}{Re}\nabla_m\mathbf{u}_m : \nabla_{-m}\bar{\mathbf{u}}_m \Bigg)\,\mathrm{d}\mathcal{V}, \quad (8)$$

where $q_m = \mathbf{u}_m\cdot\bar{\mathbf{u}}_m$, $\nabla_m f(r,z) = e^{\imath m\theta}\nabla\left(f(r,z)e^{-\imath m\theta}\right)$, and : is the dyadic double dot product operator. The left hand side of each equation represents the sum of the growth of the mode magnitude within the control volume and boundary effects. The right hand side contains the source terms resulting from viscous dissipation, non-linear interactions among perturbation modes, and focusing of perturbations by the base strain rate[37]. For each mode, the viscous dissipation always leads to a decrease in mode magnitude. The non-linear interactions of each mode can be identically matched to terms with opposite sign in other modes. Thus, while energy is transferred between modes, this mechanism does not lead to an overall increase in the strength of the perturbations. For the axisymmetric mode, this term can be related to the work required to maintain the asymmetry and tends to initially decrease the axisymmetric velocities. This energy transfer corresponds to the additional "dissipation" used by Leibovich and Kribus[16] to stabilize their axisymmetric soliton solution at large enough Reynolds numbers that viscosity alone was insufficient.

The remaining volume source term,

$$-\Re\int_{\mathcal{V}} \bar{\mathbf{u}}_m\mathbf{u}_m : \nabla_0\mathbf{U_0}\,\mathrm{d}\mathcal{V},$$

is the only term for each Fourier mode that can change the total magnitude represented by the sum of all Q_m. This term represents a focusing of asymmetric modes by the axisymmetric strain rate of the base flow and leads to perturbation growth in regions where the base flow tends to be compressing in the direction of the perturbation velocity. Thus, for near-columnar base flows which possess low strain rates, the perturbation growth is small. However, in flows containing breakdown, the region near the leading edge of the recirculation zone has large strain rates and decelerated flow both of which tend to amplify asymmetric disturbances.

3.2 Asymmetric flow evolution

In this section, we examine the transient evolution of flow asymmetries on initially axisymmetric, swirling base flows. In particular, we show that for asymmetric modes can provide a relieving effect such that non-breakdown solutions can be extended to slightly higher swirl ratios (i.e. $\Omega > \Omega_b$). Furthermore, we show how bubble modes of breakdown transform into spiral modes with the presence of asymmetries.

To examine the onset of breakdown in a flow with asymmetries, simulations are performed in Pipe A with inlet swirls larger than Ω_b. Figures 9 and 10 depict the evolution of the flow after the perturbation is introduced at the inlet. The axisymmetric base flow has an inlet swirl of 1.55, greater than $\Omega_b = 1.48$, and an axisymmetric recirculation zone exists at $t = 0$ in the test section. Figure 9 suggests that there are large oscillations in the nature of the solution beginning at about $t = 40$ non-dimensional times ($t^* W_\infty/\delta$). At this point, the asymmetries have convected to the breakdown bubble and are beginning to be amplified. This is also reflected in the temporal evolution of the minimum

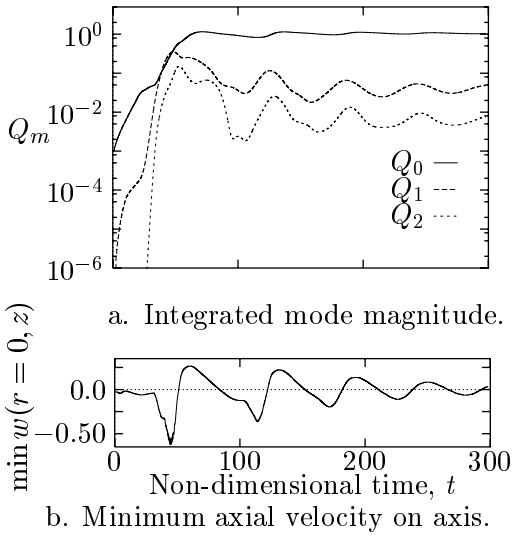

Figure 9: Development of integrated mode magnitudes and minimum axial velocity at $r = 0$ as a function of time for swirl ratio = 1.55.

axial velocity on the axis. This quantity shows large fluctuations both positive and negative as the stagnation point moves off the axis, vanishes, and reappears. These changes are also clearly evident in the instantaneous streamline images of Fig. 10. Initially, the bubble is seen to grow, both in velocity magnitude and size, with the significant asymmetric velocity confined to the recirculation zone. The asymmetries continue to grow in time such that the stagnation point is deflecting off of the $r = 0$ axis leading to the characteristic corkscrew of a spiral breakdown ($t = 60$). For $t = 80$, the flow is deflected less strongly and the strain rates decrease. This leads to a decrease in the asymmetries and the stagnation point reappears near the axis, leading again to increases in the asymmetric nature of the flow. As the stagnation point returns to the axis, the helix angle of the spiral is increased and the nearly axisymmetric bubble mode reappears ($t = 110$). This cycle continues with diminishing amplitude for a considerable time. Eventually, the solution converges to an approximately steady flow with no stagnation point. While asymmetry remains, it does not amplify significantly because of the much smaller strain rate in the axisymmetric component of the solution.

This three-dimensional solution closely resembles a continuation of the columnar solution branch that exists for purely axisymmetric flows just before breakdown. Thus, while Wang and Rusak[38] have demonstrated that axisymmetric flows with swirl ratios greater than the critical swirl ratio (*i.e.* subcritical flows) are unstable to axisymmetric disturbances, this result indicates that these flows may be stabilized by the introduction of asymmetric components. This result has also been obtained by solutions in different pipe geometries with a variety of perturbation magnitudes less than 5 percent of the base flow[37]. It appears that the additional degrees of freedom created by removing the axisymmetric constraint provides a relieving effect that allows the non-breakdown solution to be extended to at least slightly higher swirl ratios. This is consistent with the consideration of weak asymmetries as a "dissipation", provided that the mean strain rates are small enough that significant amplification of the perturbations does not occur.

Simulations at a higher swirl ratio of 1.70 show a behavior similar to the evolution described above, but after 400 non-dimensional time units, a periodic solution exists with no indication of damping. This solution oscillates between a slightly asymmetric recirculation bubble and a cork-screw vortex

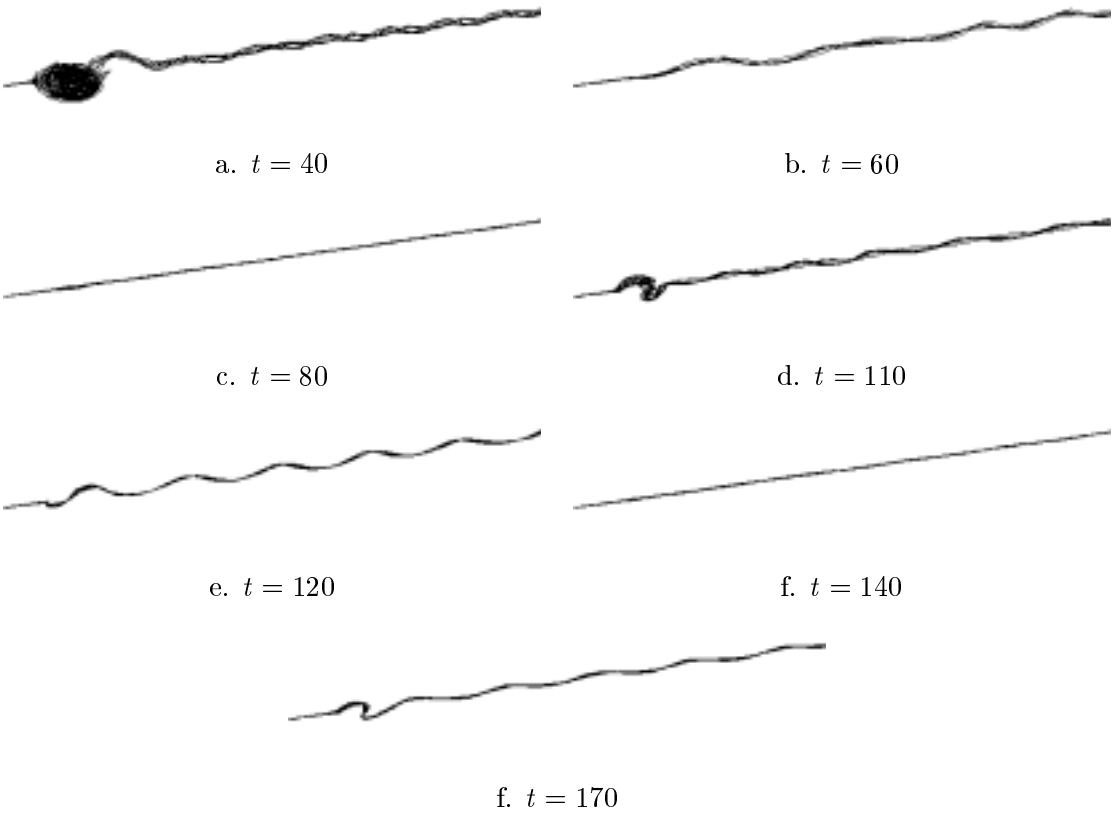

Figure 10: Instantaneous streamlines of flow after asymmetric perturbation at an inlet swirl of 1.55 in Pipe A with $Re = 500$.

core following the mechanics described above. Seven cycles with a period of about 37 non-dimensional time units were simulated with no appreciable convergence to a specific solution.

4 Summary

We have found that the onset of axisymmetric vortex breakdown in swirling pipe flows occurs when the vortex attains local criticality. Criticality was determined by solving a local eigenvalue problem for the wavenumber of standing waves on the local mean flow. Approximate determination of flow criticality using the local swirl number, while providing correct qualitative information, did not result in a unique maximum swirl number above which vortex breakdown occurs. A transient simulation of the evolution of vortex breakdown revealed that downstream-running waves are trapped approximately at the location of flow criticality. These trapped waves are slowly amplified and eventually result in a breakdown region with reversed flow and enlarged core size.

Non-axisymmetric disturbance were found to decay on base columnar base flows; however, for base flows with bubble breakdown, non-axisymmetric disturbances were amplified as a consequence of the larger strain rates that were present in the initial flow. The amplified disturbances resulted in the formation of spiral breakdown if the inlet swirl were sufficiently large. For a slightly smaller inlet swirl that would be predicted to undergo axisymmetric breakdown, near columnar solutions were found.

This suggests that the energy transfer to the asymmetric modes acts as a stabilizing influence until a sufficiently large amplitude is attained.

References

[1] D. H. Peckham and S. A. Atkinson. Preliminary results of low speed wind tunnel tests on a gothic wing of aspect ratio 1.0. CP 508, Aeronautics Research Council, 1957. 16 pp.

[2] J. H. Faler and S. Leibovich. Disrupted states of vortex flow and vortex breakdown. *The Physics of Fluids*, 20(9):1385–1400, September 1977.

[3] Turgut Sarpkaya. On stationary and travelling vortex breakdowns. *Journal of Fluid Mechanics*, 45:545–559, 1971.

[4] Christoph Brücker. Development and structural changes of vortex breakdown. Number 95-2305 in AIAA, June 1995. 26th AIAA Fluid Dynamics Conference.

[5] H. B. Squire. Analysis of the "vortex breakdown" phenomenon: Part i. Report 102, Aero. Dept., Imperial College, London, 1960. Also in *Miszellaneen der Angewandten Mechanik*, pp. 306–312, 1962. Berlin: Akademie-Verlag.

[6] A. K. Garg and Sidney Leibovich. Spectral characteristics of vortex breakdown flowfields. *Physics of Fluids*, 22(11):2053–2064, November 1979.

[7] C. Tsai and S.E. Widnall. Examination of group-velocity criterion for breakdown of vortex flow in a divergent duct. *Physics of Fluids*, 23(5):864–870, 1980.

[8] Sidney Leibovich. Vortex stability and breakdown: Survey and extension. *AIAA Journal*, 22:1192–1206, 1983.

[9] Marcel Escudier. Vortex breakdown: Observations and explanations. *Progress in Aerospace Science*, 25:189–229, 1988.

[10] M. G. Hall. Vortex breakdown. *Annual Review of Fluid Mechanics*, 4:195–217, 1972.

[11] Sidney Leibovich. The structure of vortex breakdown. *Annual Review of Fluid Mechanics*, 10:221–246, March 1978.

[12] J. M. Delery. Aspects of vortex breakdown. *Progress in Aerospace Sciences*, 30:1–59, 1994.

[13] T. Brooke Benjamin. Theory of the vortex breakdown phenomenon. *Journal of Fluid Mechanics*, 14:593–629, 1962.

[14] T. Brooke Benjamin. Some developments in the theory of vortex breakdown. *Journal of Fluid Mechanics*, 28:65–84, 1967.

[15] J. D. Randall and S. Leibovich. The critical state: A trapped wave model of vortex breakdown. *Journal of Fluid Mechanics*, 58, part 3:495–515, 1973.

[16] Sidney Leibovich and A. Kribus. Large-amplitude wavetrains and solitary waves in vortices. *Journal of Fluid Mechanics*, 216:459–504, 1990.

[17] Philip S. Beran and Fred C. Culick. The role of non-uniqueness in the development of vortex breakdown in tubes. *Journal of Fluid Mechanics*, 242:491–527, 1992.

[18] J. M. Lopez. On the bifurcation structure of axisymmetric vortex breakdown in a constricted pipe. *Physics of Fluids*, 6(11):3683–3693, November 1994.

[19] Philip S. Beran. The time-asymptotic behavior of vortex breakdown in tubes. *Computers and Fluids*, 23(7):913–937, 1994.

[20] M.G. Hall. A new approach to vortex breakdown. In *Proceedings of Heat Transfer Fluid Mechanics Inst.*, pages 319–340, La Jolla, California, 1967. University of California, San Diego.

[21] S. Wang and Z. Rusak. On the stability of an axisymmetric rotating flow. *Physics of Fluids*, 8(4):1007–1016, 1996.

[22] S. Wang and Z. Rusak. On the stability of non-columnar swirling flows. *Physics of Fluids*, 8(4):1017–1023, 1996.

[23] S. Wang and Z. Rusak. The effect of slight viscosity on near critical swirling flows. *Physics of Fluids*, 1996.

[24] S. Wang and Z. Rusak. The dynamics of a swirling flow in a pipe and transition to axisymmetric vortex breakdown. *Journal of Fluid Mechanics*, 1997.

[25] M.P. Escudier and J.J. Keller. Vortex breakdown: a two-stage transition. In *AGARD CP-342*, 1983.

[26] Z. Rusak, S. Wang, and C.H. Whiting. Numerical computations of axisymmetric vortex breakdown in a pipe. *Journal of Fluid Mechanics*, 1996.

[27] David L. Darmofal. *A Study of the Mechanisms of Axisymmetric Vortex Breakdown.* PhD thesis, Massachusetts Institute of Technology, November 1993.

[28] David L. Darmofal. Comparisons of experimental and numerical results for axisymmetric vortex breakdown in pipes. *Computers and Fluids*, 25(4):353–371, 1996.

[29] Robert E. Spall, Thomas B. Gatski, and C.E. Grosch. A criterion for vortex breakdown. *Physics of Fluids*, 30(11):3434–3440, November 1987.

[30] B. A. Robinson, R. M. Barnett, and S. Agrawal. Simple numerical criterion for vortex breakdown. *AIAA Journal*, 32(1):116–122, 1994.

[31] G.K. Batchelor. Axial flow in trailing line vortices. *Journal of Fluid Mechanics*, 20:645–658, 1964.

[32] Turgut Sarpkaya. Vortex breakdown in swirling conical flows. *AIAA Journal*, 9(9):1792–1799, September 1971.

[33] Turgut Sarpkaya. Effect of the adverse pressure gradient on vortex breakdown. *AIAA Journal*, 12(5):602–607, May 1974.

[34] J. H. Faler and Sidney Leibovich. An experimental map of the internal structure of a vortex breakdown. *Journal of Fluid Mechanics*, 86:313–335, 1978.

[35] S. Leibovich. Weakly non-linear waves in rotating fluids. *Journal of Fluid Mechanics*, 42:803–822, 1970.

[36] Andrew W. Cary, David L. Darmofal, and Kenneth G. Powell. Onset of the spiral mode of vortex breakdown. Number 97-0439 in AIAA, January 1997. 35th Aerospace Sciences Meeting.

[37] Andrew W. Cary. *The Onset of Non-Axisymmetric Vortex Breakdown.* PhD thesis, University of Michigan, Ann Arbor, MI, August 1997.

[38] S. Wang and Z. Rusak. On the stability of an axisymmetric rotating flow in a pipe. *Physics of Fluids*, 8:1007–1016, 1996. Also as RPI Aeronautical Engineering Report 108.

Paper: 16
Author: Dr. Darmofal

Question by Dr. Greenwell: What is the effect of the tube wall constraint on the structure (and stability) of the breakdown. Specifically, do stable, closed bubbles form in unconstrained vortex flows?

Answer: At this point, we do not know. For the pipe flow, we have found that spiral breakdown is the final form for all of the simulations we have performed. But, even this conclusion is based on swirls that are only slightly (10-20%) higher than the critical swirl for axisymmetric breakdown.

Question by Dr. Mitchell: Have you studied other vortex models beyond Burgers' vortex model? With delta wings, experiments have shown a trend to have a vortex different from that demonstrated by Burgers' vortex.

Answer: Yes. We have looked a less physical models (such as the Rankine vortex with a plug flow axial velocity) as well as profiles from experimental data. The conclusions are quite similar.

This page has been deliberately left blank

Page intentionnellement blanche